Tracing multi-anthropogenic inputs in intertidal mudflat sediments using lead and zinc isotopes

Sanny Castro, Wanilson Luiz-Silva, Hyeryeong Jeong, João Barreira, Wilson Machado, Christian Sanders, Jeremie Garnier, Daniel Ferreira Araujo

Marine Pollution Bulletin 227 (2026) 119470

Contents lists available at ScienceDirect

Marine Pollution Bulletin

journal homepage: www.elsevier.com/locate/marpolbul

Tracing multi-anthropogenic inputs in intertidal mudflat sediments using lead and zinc isotopes☆

Sanny Castro [a], Wanilson Luiz-Silva [a], Hyeryeong Jeong [b], João Barreira [c,d], Wilson Machado [d], Christian Sanders [e], Jeremie Garnier [f], Daniel F. Araújo [b,*]

[a] Institute of Geosciences, State University of Campinas (UNICAMP), Campinas, SP, 13083-855, Brazil
[b] Ifremer, CCEM – Unité Contamination Chimique des Écosystèmes Marins (CCEM), F-44000, Nantes, France
[c] Université d'Angers, Nantes Université, Le Mans Université, CNRS, UMR 6112, Laboratoire de Planétologie et Géosciences, Angers, France
[d] Department of Geochemistry, Fluminense Federal University (UFF), Niterói, RJ, 24020-141, Brazil
[e] National Marine Science Centre, Southern Cross University, PO Box 4321, Coffs Harbour, NSW, 2450, Australia
[f] Institute of Geosciences, University of Brasília (UnB), Graduate Program in Geology, Brasília, DF, 70910-900, Brazil

ARTICLE INFO

Keywords:
Mangrove
Pb isotopes
Zn isotopes
Marine pollution
Industrial contamination
Sediment core
Trace metal

ABSTRACT

Intertidal mudflat sediments are valuable archives of long-term contamination in tropical estuaries, yet isotopic approaches remain underexplored in these environments. In this study, we present new Pb ($^{208}Pb/^{206}Pb$, $^{206}Pb/^{207}Pb$) and Zn ($\delta^{66}Zn$) isotopic records integrated with previously published Pb and Zn concentration data from a sediment core collected in the Santos–Cubatão Estuarine System (southeastern Brazil), reconstructing the history of contamination in one of the most industrialized coastal areas in Latin America. Pb isotopic ratios clearly separate deeper pre-industrial sediments with geogenic signatures from upper layers influenced by radiogenic Pb inputs associated with emissions from a steel plant. Zn isotopic compositions reveal temporal shifts in contamination: heavier $\delta^{66}Zn$ values correspond to high-temperature industrial processes, whereas lighter values after the mid-1980s reflect increasing contributions from diffuse urban effluents following the implementation of environmental controls. Importantly, isotopic data capture early anthropogenic signals of contamination in sediment layers where elemental concentrations alone still resembled geogenic background conditions. These findings demonstrate that Pb and Zn isotopes provide sensitive tracers of shifting contamination sources, enabling a refined reconstruction of pollution history in mudflats beyond what concentration data can reveal. This study underscores the potential of isotope geochemistry to improve legacy pollution assessments in estuarine systems worldwide.

1. Introduction

Estuaries rank among the most productive and valuable coastal ecosystems on Earth, providing key services such as shoreline stabilization, carbon sequestration, nutrient cycling, and nursery habitats for marine life. However, they are also among the most vulnerable coastal environments, particularly in regions subjected to intense urbanization and industrialization. Due to their fine-grained sediments and high organic matter content, mangrove and mudflat environments act as efficient sinks for contaminants, preserving stratigraphic records that integrate both natural processes and human influence. As a result, estuarine sediments are increasingly recognized as natural archives capable of recording the intensity and chronology of environmental contamination over decadal to centennial timescales (Lonsdale et al., 2022; Castro et al., 2021; Guo et al., 2025). Among the contaminants accumulated in these environments, trace metals such as lead (Pb) and zinc (Zn) are of particular concern due to their persistence, toxicity, and widespread association with industrial and urban activities. In human-impacted coastal systems, Pb and Zn are commonly enriched due to multiple and overlapping pathways, including riverine transport, atmospheric deposition, tidal exchange, and direct industrial and urban effluents. However, interpreting bulk metal concentrations alone is often insufficient to disentangle natural background inputs from superimposed anthropogenic contributions, especially in estuaries with

☆ This article is part of a Special issue entitled: 'Source Apportionment' published in Marine Pollution Bulletin.

* Corresponding author.
E-mail address: daniel.ferreira.araujo@ifremer.fr (D.F. Araújo).

https://doi.org/10.1016/j.marpolbul.2026.119470
Received 6 November 2025; Received in revised form 3 February 2026; Accepted 23 February 2026
Available online 3 March 2026

long histories of industrialization and complex source mixtures (Dong et al., 2015; Obrist et al., 2018; Hossain et al., 2024).

To overcome these limitations, isotopic geochemistry has emerged as a powerful tool for environmental provenance and source apportionment (Pontér et al., 2020; Krupnova et al., 2023). Radiogenic Pb isotopes (^{206}Pb, ^{207}Pb, ^{208}Pb) behave conservatively in the environment and retain information on the geological age and origin of source materials. Variations in Pb isotopic ratios allow discrimination between geogenic inputs derived from crustal weathering and anthropogenic emissions associated with metallurgical activities, fossil fuel combustion, and industrial processes (Sun et al., 2011; Yu et al., 2021; Fangwen et al., 2025). In contrast, stable Zn isotopes (^{64}Zn, ^{66}Zn, ^{67}Zn, ^{68}Zn) undergo measurable fractionation during both high-temperature industrial processes (e.g., ore smelting and refining) and low-temperature biogeochemical reactions such as sorption, dissolution, and organic complexation (Araújo et al., 2017, 2018; Garnier et al., 2024). This dual sensitivity makes Zn isotopes particularly valuable for tracing metallurgical inputs, urban effluents, and post-depositional metal cycling in sediments (Araújo et al., 2019; Jeong and Ra, 2021; Jeong et al., 2023). Despite these advances, combined Pb—Zn isotopic applications in estuarine environments, particularly in tropical regions, remain relatively scarce (Junqueira et al., 2024).

The Santos–Cubatão Estuarine System (southeastern Brazil) represents one of the most emblematic examples of long-term industrial impact on a tropical coastal environment. Since the 1950s, the region has hosted one of the largest petrochemical and steelmaking complexes in Latin America (Couto, 2003), and estuarine sediments show elevated concentrations of Pb, Zn, and other trace metals, reflecting legacy contamination and diffuse urban inputs (Luiz-Silva et al., 2008). This setting contributes to persistent contamination and ongoing impacts on water quality and estuarine biota, highlighting that metal contamination in the Santos–Cubatão Estuarine System remains a current and pressing environmental concern (Angeli et al., 2021). Continued industrial growth and rapid urbanization have intensified metal inputs, whose sources remain poorly resolved. In this study, we address this knowledge gap by presenting the first combined Pb and Zn isotopic dataset for sediments from the Santos–Cubatão Estuarine System. A sediment core was analyzed for Pb (^{206}Pb/^{207}Pb and ^{208}Pb/^{206}Pb) and Zn ($\delta^{66}Zn_{JMC}$) isotopic compositions, which were integrated with previously published elemental concentration data (Luiz-Silva et al., 2008), to reconstruct the temporal evolution of contamination sources. The specific objectives were to: (i) establish baseline isotopic signatures in pre-industrial sediments; (ii) identify isotopic shifts associated with industrial emissions during peak industrialization; and (iii) detect transitions toward diffuse urban sources following the implementation of environmental regulations.

2. Study area and geological background

The Santos–Cubatão Estuarine System (SE Brazil; Fig. 1) comprises an interconnected network of rivers, tidal channels, mudflats, and extensive mangrove ecosystems, all of which ultimately drain into Santos Bay (Mahiques et al., 2016). The estuarine complex is located at the foot of the Serra do Mar mountain range, one of the most prominent geomorphological features along the southeastern Brazilian coast. The mountainous sector is predominantly covered by Atlantic Forest (*Mata Atlântica* biome) vegetation, whereas the low-lying estuarine plain hosts well-developed mangrove ecosystems. Both environments are legally protected, reflecting their high ecological value and environmental sensitivity.

The regional geology (Fig. 1) is dominated by Precambrian crystalline basement rocks of the Coastal Complex, comprising Neoproterozoic medium- to high-grade metamorphic rock assemblages. These include metasedimentary rocks such as schists, paragneisses, and quartzites, as well as orthoderived lithologies represented by orthogneisses, gneisses, and migmatites. Mylonites associated with the Cubatão shear zone (Cubatão Fault) are also present. Locally, this basement is intruded by Neoproterozoic granitic bodies (Almeida and Carneiro, 1998; Perrotta et al., 2005). Together, these lithologies represent reworked crustal domains formed during successive Proterozoic orogenic cycles, resulting in a structurally complex framework characterized by heterogeneous crustal ages and strong tectonic inheritance. Weathering and erosion of the crystalline basement constitute the primary natural source of terrigenous material and geogenic trace metals supplied to the

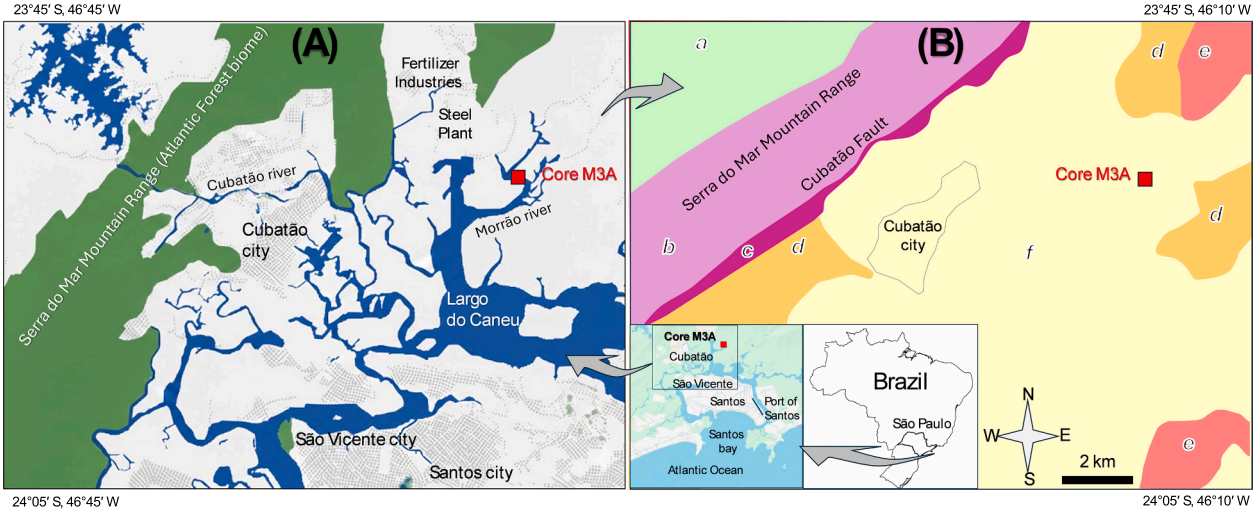

Fig. 1. (A) Location of the Santos–Cubatão Estuarine System, southeastern Brazil. The red square indicates the sampling site of sediment core M3A in the Morrão River mangrove (23°52′36″ S; 46°21′27″ W), located near of fertilizer and steel industries. Rivers and estuarine channels are shown, together with the Atlantic Forest biome (green), the cities of Cubatão, São Vicente, and Santos.
(B) Simplified geological framework of the study area based on the Geological Map of the State of São Paulo (scale 1:750,000; Perrotta et al., 2005). The Precambrian crystalline basement (Complexo Costeiro) comprises metasedimentary rocks, including schists, paragneisses, and quartzites (unit *a*), and orthoderived rocks, including orthogneisses (*b*), mylonites (*c*) associated with the Cubatão shear zone (fault), and gneisses and migmatites (*d*). Neoproterozoic granitic intrusions are locally exposed (*e*). Quaternary sedimentary deposits (*f*) include fluvial, fluvio-lagoonal, estuarine, and coastal sediments forming the Santos–Cubatão coastal plain, characterized by dense mangrove vegetation. The two inset panels illustrate the location of the study area within Brazil and along the São Paulo coastline, highlighting the Port of Santos and Santos Bay. (For interpretation of the references to colour in this figure legend, the reader is referred to the web version of this article.)

Santos–Cubatão Estuarine System.

Climatically, the region is influenced by the interaction of subtropical, polar, and equatorial air masses, resulting in high annual humidity (70–90%) and intense orographic rainfall along the *Serra do Mar*. Mean temperatures range from approximately 18 °C in the mountainous areas to about 25 °C along the coastal plain (Klumpp et al., 1996). These conditions promote intense chemical weathering, enhancing the mobilization of lithogenic elements from the crystalline basement into the estuarine sediments.

From the mid-20th century onward, the natural geochemical background of the Santos–Cubatão Estuarine System has been increasingly overprinted by anthropogenic inputs. Since the 1950s, the region has hosted one of the largest industrial complexes in Latin America, including petrochemical facilities (from 1955), a chlor-alkali plant (1964), a steel plant (1966), and fertilizer industries producing phosphate- and nitrogen-based products from the 1970s onward (Couto, 2003). The legacy of this industrialization is well documented in sediments, waters, atmosphere, and biota, with elevated concentrations of multiple trace metals, particularly Zn and Pb (Luiz-Silva et al., 2006; Borrely et al., 2018; Angeli et al., 2021). Although industrial discharges were substantially reduced following the implementation of government-led pollution control programs in the 1980s, metal concentrations in estuarine sediments remain above natural background levels. This persistence reflects the combined effects of legacy contamination, ongoing diffuse urban inputs, and sediment remobilization associated with dredging and operations at the Port of Santos (Castro et al., 2021). In this context, the combined influence of geogenic inputs derived from the weathering of Precambrian basement rocks and anthropogenic contributions from industrial and urban sources makes the Santos–Cubatão Estuarine System particularly suitable for isotopic investigations aimed at disentangling natural and human-induced metal sources.

3. Materials and methods

A sediment core (M3A) was collected from a mudflat located at the seaward fringe of the mangrove, within the intertidal zone of the Morrão River (23°52′36" S; 46°21′27" W; Fig. 1). The sampling site is periodically exposed during low tide, with a maximum tidal range of approximately 1.5 m during spring (syzygy) tides. This area is directly influenced by effluents from a fertilizer plant and a steel factory located upstream (Luiz-Silva et al., 2008). The core was retrieved using a PVC tube manually inserted into the sediment to a total depth of 260 cm. In the laboratory, the core was sectioned into 5 cm intervals down to a depth of 60 cm and 10 cm intervals below 60 cm, and sediments adhering to the tube walls were discarded to avoid contamination (Fig. S1).

Concentrations of Pb, Zn, Fe, and Al, together with sediment grain-size distribution, organic matter content, and chronological markers along the M3A core, were obtained from Luiz-Silva et al. (2008). In that study, sediment samples from the same core were oven-dried (50 °C), ground in an agate mill, and digested using a mixed acid solution (H_2O: HF:$HClO_4$:HNO_3, 2:2:1:1). Approximately 0.25 g of powdered sediment was heated to dryness on a hot plate, followed by re-dissolution in 50% HCl and final dilution to 10 mL with 5% HCl. Elemental concentrations were determined by ICP-MS (PerkinElmer ELAN 6000). Analytical accuracy was assessed through the repeated analysis of a certified reference material (LKSD-3, CANMET) and an in-house standard (DST6), processed using the same digestion protocol as the samples. Recoveries for Pb and Zn were within acceptable analytical ranges, as reported in Table S1 of Luiz-Silva et al. (2008). Replicate analyses ($n = 4$) were performed for quality control, confirming the stability and reproducibility of the measurements. Grain-size distribution was determined by laser diffraction (CILAS 1090 L) after dispersing bulk sediment (1 g) in 30 mL of an aqueous sodium hexametaphosphate solution (40 g L^{-1}) and mechanically shaking the suspension for 24 h. Organic matter content was estimated by loss on ignition at 550 °C for 4 h. These previously published datasets provide the geochemical and sedimentological framework required to interpret the novel Pb and Zn isotopic data presented in this study.

For isotope analysis, a second set of dry powder aliquots of the same samples was processed at the *Unité de Contamination Chimique des Ecosystèmes Marins* (Ifremer, Nantes, France) in 2023. Firstly, samples were digested using an acid digestion method with a mixed solution of H_2O, HF, and HNO_3. Then, aliquots of the final solution were taken for isotope measurements. Lead isotope ratios ($^{206}Pb/^{207}Pb$ and $^{208}Pb/^{206}Pb$) were determined using a Thermo Fisher Scientific TQ-ICP-MS (Germany). Analytical accuracy and precision were assessed through repeated measurements of the NIST SRM-981 lead standard, following the procedures described in Sun et al. (2011) and Yu et al. (2021). Mass bias and instrumental drift were corrected by sample–standard bracketing (Todt et al., 1996). Internal relative standard deviations averaged 0.20 ± 0.07% for $^{206}Pb/^{207}Pb$ and 0.47 ± 0.17% for $^{208}Pb/^{206}Pb$ (1σ, $n = 60$), consistent with reproducibility reported in previous Pb isotope studies (Hu et al., 2011; Fangwen et al., 2025). The accuracy of the analytical procedure was further verified through parallel measurements of the sediment reference material (MESS-4). No significant instrumental drift or matrix effects were detected during the analytical runs. Measured Pb isotope ratios for NIST SRM-981 and MESS-4 and their comparison with recommended literature values are reported in Table S1.

Zinc isotope compositions were determined using a Thermo Fisher Scientific Neptune multi-collector MC-ICP-MS equipped with a low-flow PFA nebulizer at *Pôle Spéctrometrie Océan (PSO, Ifremer, Plouzané)*. Prior to isotopic analysis, Zn was chemically separated from the sample matrix by anion-exchange chromatography following the protocol described in Araújo et al. (2017, 2018, 2019). Aliquots containing 2–4 μg of Zn were loaded onto Bio-Rad PolyPrep columns filled with AG-MP1 anion-exchange resin (100–200 mesh) in a HCl medium. Matrix elements were eluted using 2 M HCl, and Zn was subsequently recovered using 0.5 M HNO_3. The purified Zn fractions were evaporated to dryness and re-dissolved in 2% HNO_3 prior to MC-ICP-MS analysis. Zinc recovery yields were systematically monitored by ICP-MS measurements of pre- and post-column solutions and averaged 99 ± 7%, consistent with previous applications of this method (Araújo et al., 2017, 2019). Total procedural blanks (digestion + chromatography) were below 30 ng and represented <1% of the Zn content of the samples. Potential matrix effects were assessed by monitoring residual matrix elements after purification and by ensuring identical Zn concentrations between samples and standards during analysis. No significant matrix-induced mass bias or signal suppression was detected.

Isotopic compositions are reported as $\delta^{66}Zn_{JMC}$ relative to the JMC-Lyon reference standard according to the following equation:

$$\delta^{66}Zn_{JMC}\left(‰\right) = \left(\frac{\left(^{66}Zn/^{64}Zn\right)_{sample}}{\left(^{66}Zn/^{64}Zn\right)_{JMC}} - 1\right) \times 1000 \quad (1)$$

Analytical accuracy and precision were evaluated through repeated measurements of the standard reference JMC-Lyon and the reference material (MESS-4), during analytical runs in the sample–standard bracketing mode (Araújo et al., 2017; Garnier et al., 2024). Reproducibility was typically better than ±0.05‰ (2σ, $n = 15$), and accuracy was confirmed by matching the values of $\delta^{66}Zn_{JMC}$ obtained for MESS-4 (0.23 ± 0.05‰, 2σ, $n = 4$ replicates) with those in the literature (0.26 ± 0.02, 2σ; Jeong et al., 2021).

To account for grain-size and mineralogical variability, enrichment factors (EF) for Pb, Zn, and Fe were calculated using Al as a conservative normalizer (Salomons and Förstner, 1984):

$$EF = \frac{(M/Al)_{sample}}{(M/Al)_{background}} \quad (2)$$

where *M* represents the element of interest (Pb, Zn, or Fe) and Al is the normalizing element. Background concentrations were defined using the lower (>220 cm depth), pre-industrial section of the same sediment core (Luiz-Silva et al., 2008). Basic statistical analyses were performed using the XSTAT software package.

4. Results and discussion

4.1. Geochronology, metal enrichments, and baselines

Fig. 2 highlights key geochronological events recorded in the core, particularly the construction of the steel plant between 1959 and 1963 (with low production until 1976), the onset of high steel production after 1976, and the implementation of contamination-control measures in 1984 to reduce untreated effluent discharges into the Santos–Cubatão Estuarine System. The depth–time framework adopted for core M3A follows the chronology and sedimentation-rate constraints reported by Luiz-Silva et al. (2008); Fig. 3; Table S2). Accordingly, the attribution of 110 cm to ~1976 should be regarded as an approximate estimate, with uncertainty reflecting temporal variability in sediment accumulation rates in this intertidal mudflat setting. Fertilizer industry operations began in 1976; however, the steel plant has been identified as the dominant primary anthropogenic source of Pb and Zn to the estuary. The iron ore processed at this facility is sourced from banded iron formations (BIFs) of the Quadrilátero Ferrífero, Minas Gerais State, Brazil (Luiz-Silva et al., 2008), providing a geogenic reference framework for interpreting metal inputs along the core.

Within this chronological framework, the sediments along the core were predominantly fine-grained (Fig. 3; Table S2), with a clay–silt fraction of 91.0 ± 13.5 vol%, and organic matter content remained relatively uniform, averaging 11.7 ± 1.39 wt%. The notably high sedimentation rate in core M3A, located in a mudflat, reached up to 7.6 cm yr^{-1} of vertical accretion (Fig. 2), which may result from a combination of anthropogenic activities and landslides in the Serra do Mar escarpments (Luiz-Silva et al., 2008).

Additionally, Table S2 presents Fe (total), Al, Pb, and Zn data reported by Luiz-Silva et al. (2008). Lead and Zn concentrations ranged from 27.3 to 325 mg kg^{-1} and from 85.4 to 929 mg kg^{-1}, respectively, with enrichment factors (EF) varying from ~1 to 20 for both metals (Fig. 2). Iron concentrations ranged from 4.59 to 32.5 wt%, with EF values between ~1 and 18.9. Higher concentrations and EF values for these metals occur from approximately 110 cm depth (~1976) to the top of the core, whereas lower concentrations characterize the deeper sections, where geochemical background conditions are established below ~220 cm depth (prior to steel plant construction; Fig. 2). Additional data from Luiz-Silva et al. (2008) indicate that Al (Table S2), used as a conservative lithogenic element for EF calculations, shows relatively constant concentrations throughout the core, averaging 7.69 ± 1.90 wt %.

To evaluate the integrity of this geochemical record, because the core was collected in an intertidal mangrove–mudflat setting, potential sediment mixing driven by tidal processes must be considered. Although tidal currents may promote short-term sediment redistribution at the

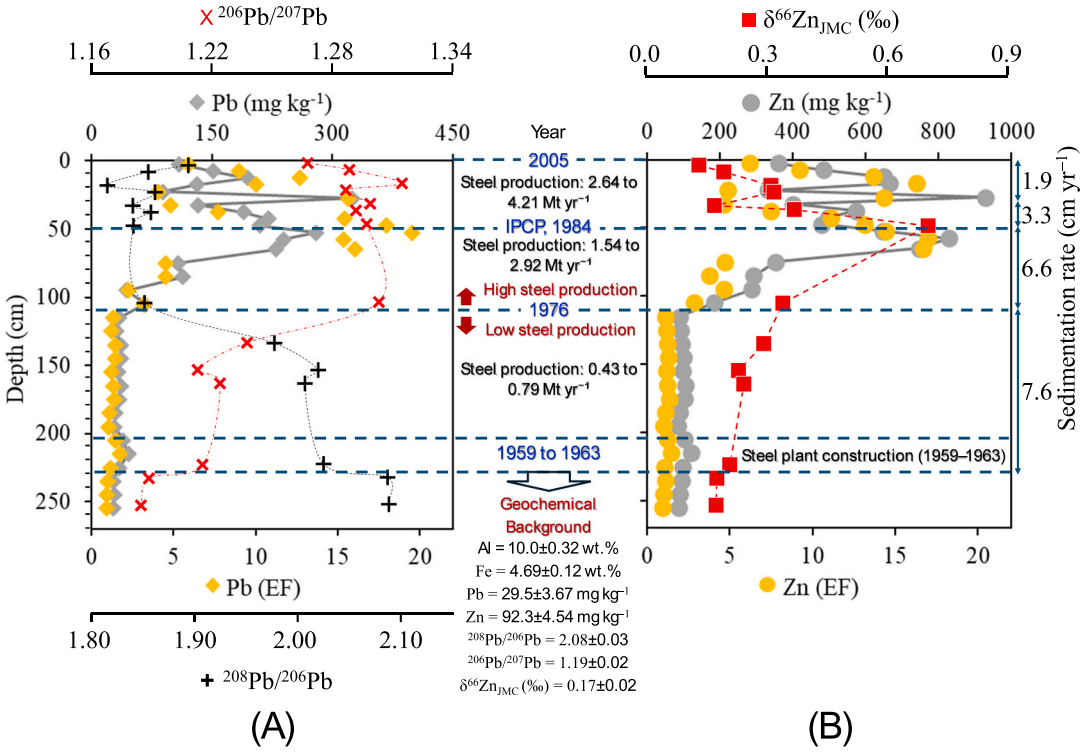

Fig. 2. Depth profiles of Pb (A) and Zn (B) in the Morrão River sediment core (M3A). In panel (A), grey diamonds represent Pb concentrations, yellow diamonds indicate Pb enrichment factors (EF), red crosses show $^{206}Pb/^{207}Pb$ ratios, and black crosses correspond to $^{208}Pb/^{206}Pb$ ratios. In panel (B), grey circles represent Zn concentrations, yellow circles indicate Zn EF, and red squares show $\delta^{66}Zn_{JMC}$ values. Horizontal dashed lines indicate key chronological milestones: construction of the steel plant (1959–1963), low-production phase (1963–1976), high-production periods (1977–1984 and 1985–2004), and the implementation of Pollution Control Policies (IPCP - 1984). The lowermost interval of the core (220–250 cm) is interpreted as the geochemical background. All data, except Pb and Zn isotopes (this study), were sourced from Luiz-Silva et al. (2008). Sedimentation rates reported by these authors are shown and provide the basis for the approximate depth–age framework used in this study. Quality assurance and quality control (QA/QC): relative percentage differences for Pb and Zn analyses, based on four replicates, were better than 8%; analytical uncertainties (2σ) were better than 0.03 for Pb isotope ratios and 0.07‰ for $\delta^{66}Zn_{JMC}$. (For interpretation of the references to colour in this figure legend, the reader is referred to the web version of this article.)

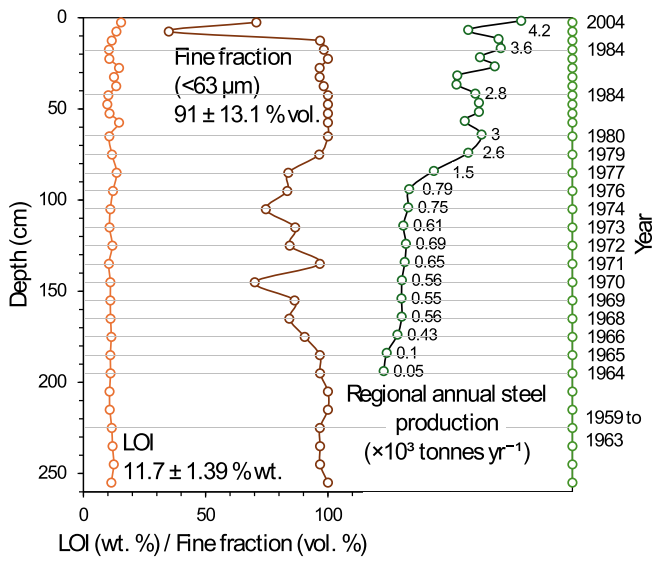

Fig. 3. Depth profiles of loss on ignition (LOI, wt%), fine-grained fraction (<63 μm, vol%), and regional annual steel production ($\times 10^3$ t yr^{-1}) for sediments from the Morrão River core (M3A; Santos–Cubatão Estuarine System, SE Brazil). Depth (cm) and corresponding calendar years are shown along the vertical axis, based on the established age–depth model. Grain-size and LOI data illustrate the sedimentary characteristics of the core, whereas regional annual steel production is presented as contextual information supporting the interpretation of anthropogenic influence. Granulometric data, LOI values, steel production records, and age–depth correspondence were compiled from Luiz-Silva et al. (2008).

sediment–water interface, the dominance of fine-grained deposits and the consistency of lithogenic tracers along the core indicate that sediment provenance remained broadly stable over time. Previous studies further support that sediment inputs are primarily of local fluvial and estuarine origin rather than oceanic. Using radionuclide tracers ($^{239+240}$Pu), Sanders et al. (2014) demonstrated steady and continuous sediment accretion in mangrove cores collected at both lower and upper tidal elevations located approximately 150 m from the core analyzed in this study, with accretion rates of ~6.7 mm yr^{-1}. In addition, these authors showed that enriched $\delta^{13}C$ values reflect increased contributions from planktonic and benthic algal material, whereas elevated $\delta^{15}N$ values indicate inputs from urban and industrial effluents and associated nitrogen cycling under eutrophic conditions. Despite tidal influence, these isotopic records display coherent downcore trends, demonstrating continuous vertical accretion and limited sediment reworking by marine currents. Overall, these observations support the interpretation that the sedimentary archive in the study area reliably preserves temporal changes in contaminant sources.

4.2. Geogenic and anthropogenic lead and zinc isotopic signatures

Lead and zinc isotopic compositions varied systematically along the core (M3A), recording the transition from a geogenic background to intense industrial activity (Fig. 2, Table S2). In the deepest section (>220 cm), defined as the geochemical background, $^{208}Pb/^{206}Pb$ ratios (~2.08) and $^{206}Pb/^{207}Pb$ ratios (~1.19) remained stable, likely associated with natural inputs from regional lithologies. Correspondingly, $\delta^{66}Zn_{JMC}$ values were uniform (~0.17‰), establishing the isotopic baseline for pre-industrial sediments. At 225 cm, coinciding with the steel plant construction period (1959–1963), Pb isotopes began to deviate from background values, with $^{208}Pb/^{206}Pb$ decreasing to 2.02 and $^{206}Pb/^{207}Pb$ increasing to 1.22. A slight $\delta^{66}Zn$ enrichment (0.20‰) also marked the initial anthropogenic influence. Between 165 and 135 cm, corresponding to the period of low steel production, $^{208}Pb/^{206}Pb$ ratios declined further (2.02–1.98), while $^{206}Pb/^{207}Pb$ ratios increased (1.21–1.24). In addition, increasing $\delta^{66}Zn$ values (0.23–0.30‰) suggest a mixed signal reflecting contributions from both the geogenic background and low steel plant production. As shown in Fig. 2 and Table S2, despite industrial activities occurring concurrently with sedimentation during this period (low steel production), the concentrations of Pb and Zn (and their respective enrichment factors) are uniform from 110 cm down to the base of the core, except for a small peak at approximately 220 cm, which corresponds to the period of steel plant construction. By contrast, over the same interval, Pb and Zn isotopic signatures appear to be more sensitive indicators of the onset of industrial activity than bulk concentrations, even when such activity occurred at a relatively small scale.

Following this initial anthropogenic signal, the onset of abrupt changes in isotopic ratios is observed from the 110 cm depth horizon onward (corresponding to ~1976), where $^{208}Pb/^{206}Pb$ decreased to 1.85, $^{206}Pb/^{207}Pb$ increased to 1.30, and $\delta^{66}Zn$ rose to 0.35‰. This depth marks the transition from low to high industrial activity, simultaneously captured by both Pb and Zn isotopic systems. The upper section of the core (0–50 cm, 1976–2005) was deposited during peak steel production and is characterized by a persistent industrial Pb isotopic signature, whereas Zn isotopes record more variable inputs reflecting additional non-metallurgical sources (see below). The $^{208}Pb/^{206}Pb$ ratios (average 1.85 ± 0.02) and $^{206}Pb/^{207}Pb$ ratios (average 1.29 ± 0.01) show limited variability and largely reproduce the isotopic values established at the onset of intensified industrial activity after 1976.

4.3. Geochemical affinities

In most estuarine systems, trace metals are strongly associated with fine-grained particles and organic matter (Tang et al., 2018). In contrast, in the study area, no significant correlations were found between silt–clay contents and Pb or Zn concentrations, nor with their isotopic signatures ($^{206}Pb/^{207}Pb$, $^{208}Pb/^{206}Pb$, $\delta^{66}Zn_{JMC}$; all $|r| < 0.05$, $p > 0.05$) (Table S3). Organic matter also showed no meaningful relationships, except for $\delta^{66}Zn_{JMC}$, which exhibited a weak negative trend ($r = -0.54$). The absence of correlations or the presence of negative correlations suggests that the high organic matter input in the study area may act as a diluting factor on metal concentrations, depending on the predominance of organic matter sources over time, as previously observed in this system (Machado et al., 2016). Such behavior makes the Santos–Cubatão estuarine system, particularly in the Morrão River domain, a less typical case when compared to other contaminated estuaries.

In addition, no statistically significant correlations were observed between $\delta^{66}Zn_{JMC}$ and Pb isotope ratios ($|r| \approx 0.45$, $p > 0.05$; Table S3), suggesting that the Zn and Pb isotopic systems evolved largely independently within the core. By contrast, strong correlations between Pb ($r = 0.79$, $p < 0.05$) and Zn ($r = 0.74$, $p < 0.05$) concentrations and Fe are mirrored in the isotopic data. Specifically, $^{208}Pb/^{206}Pb$ ($r = -0.64$, $p < 0.05$), $^{206}Pb/^{207}Pb$ ($r = 0.62$, $p < 0.05$), and $\delta^{66}Zn_{JMC}$ ($r = 0.72$, $p < 0.05$) exhibit strong relationships with Fe (Table S3). These results underscore the significance of Fe-bearing phases, possibly extending beyond oxyhydroxides, in influencing trace-metal distributions and isotopic signatures. Iron concentrations are anomalously high in the area due to steel plant contamination (up to 32.5 wt%; Table S2), partitioned among magnetite and hematite (dominant phases), as well as vivianite and pyrite (Volpato, 2015). Their stability is strongly influenced by redox conditions: Fe^{2+} phases, such as vivianite, pyrite, and magnetite, are favored under suboxic to reducing environments, whereas Fe^{3+} phases, including hematite and minor magnetite, predominate under oxic conditions. Under most geochemical conditions, heavier Zn isotopes tend to be preferentially incorporated into Fe-bearing phases (Araújo et al., 2017; Garnier et al., 2024), which explains the strong positive correlation observed between Fe and $\delta^{66}Zn_{JMC}$. This pattern underscores the dual role of Fe-bearing phases, including vivianite, a hydrated Fe-phosphate mineral that plays a more important role in coastal sediments than previously recognized

(Kubeneck et al., 2021), as both geochemical barriers and isotopic fractionation agents in estuarine systems.

In general, lead isotopic ratios remain conservative during adsorption processes (Sun et al., 2011; Yu et al., 2021), indicating that Fe phases primarily act as sinks without inducing isotopic fractionation. The relationship between Pb isotopic ratios and Fe (Table S3), marked by a decrease in $^{208}Pb/^{206}Pb$ and a concomitant increase in $^{206}Pb/^{207}Pb$ toward the top of the core (Fig. 2; Table S2), is interpreted as reflecting mixing between isotopically lighter Pb derived from iron ore processing at the steel plant and geogenic Pb signatures preserved in deeper sediment layers. Because the iron ore supplied to the steel plant in the study area was sourced from BIFs of the Quadrilátero Ferrífero, the Pb isotopic signature of the ore was inferred from Pb isotope data measured directly in hematite-rich iron formations that constitute the source of the material processed at the steel plant (Cauê Formation; Olivo et al., 1996; Table S4). Data from mixed hematite in itabirite rocks ($^{208}Pb/^{206}Pb \approx 0.61$; $^{206}Pb/^{207}Pb \approx 3.29$) and jacutinga rocks ($^{208}Pb/^{206}Pb \approx 0.82$; $^{206}Pb/^{207}Pb \approx 2.56$) indicate strong radiogenic enrichment in ^{206}Pb. This ore-related signature is consistently recorded along the M3A core, with ^{206}Pb-enriched compositions becoming increasingly pronounced as steel plant residues were discharged more intensively into the estuarine system.

4.4. Isotopic fingerprints of Pb and Zn

The Pb isotopic ratios along the core reveal a clear two-endmember system (Fig. 4). The first endmember, recorded in lower sediments (>110 cm depth; pre-1976), is characterized by relatively low $^{206}Pb/^{207}Pb$ ratios (1.19–1.24) and high $^{208}Pb/^{206}Pb$ ratios (1.98–2.08), corresponding to background conditions dominated by geogenic inputs and limited industrial activity. These values overlap with natural isotopic signatures reported for unpolluted Atlantic sediments (Barros de Oliveira et al., 2009) and the Upper Continental Crust (Millot et al., 2004). Comparable isotopic signatures have also been reported for other unpolluted environments, although not shown in Fig. 4, such as Sepetiba Bay (Jeong et al., 2023) and Fernando de Noronha Island (Barros de Oliveira et al., 2009). In addition, gneiss samples collected in São Paulo city (approximately 52 km from the study area), lithologically comparable to the Serra do Mar gneisses, exhibit Pb isotopic compositions within the range expected for crustal sources, with $^{206}Pb/^{207}Pb$ ratios of 1.100 ± 0.002 (1σ) and $^{208}Pb/^{206}Pb$ ratios of 2.197 ± 0.007 (1σ; Aily, 2001). Taken together, these observations suggest that the deeper sediments analyzed predominantly reflect Pb derived from the weathering of crustal rocks, consistent with a geogenic isotopic signature associated with mixed geological ages, as described for natural Pb backgrounds (Komárek et al., 2008).

By contrast, the second endmember, represented by the upper sediments (0–110 cm), exhibits more radiogenic $^{206}Pb/^{207}Pb$ ratios (1.27–1.32) and lower $^{208}Pb/^{206}Pb$ ratios (1.82–1.89; Fig. 4). These isotopic signatures fall within the broad range reported for industrial Pb emissions, particularly in terms of $^{206}Pb/^{207}Pb$ ratios, including smelter-related materials and metallurgical dusts (Rabinowitz, 2002, 2005). Comparable Pb isotopic fields have been documented in urban and industrially impacted sediment cores, where shifts toward more radiogenic $^{206}Pb/^{207}Pb$ values reflect temporal changes in anthropogenic Pb inputs (Hu et al., 2011). However, Pb isotopic compositions in metallurgical products and associated emissions can vary substantially depending on ore provenance, blending of raw materials, and processing history, as widely reported in coastal and urban sediment studies (Cunha et al., 2018; Hu et al., 2011). Accordingly, the isotopic signatures recorded in the upper sediments likely reflect a mixture of industrial Pb sources, as outlined above, rather than a distinct fingerprint of individual slags or ingots. The atmospheric particulate matter from the study area (Fig. 4) serves as a relevant indicator, as its Pb isotopic signatures span both the geogenic and anthropogenic fields, supporting a mixed contribution of regional crustal Pb and metallurgical–related emissions.

In comparison with the Pb system, Zn isotopes add further complexity to the system, revealing three main isotopic clusters (Fig. 5): (i) bottom sediments (>110 cm depth; pre-1976), with relatively light $\delta^{66}Zn_{JMC}$ values (0.16 to 0.30‰), consistent with Bulk Silicate Earth lithologies and pristine mangrove environments (Chen et al., 2013; Garnier et al., 2024); (ii) post-1976 sediments (<110 cm depth) from the intermediate to upper sections, showing progressively heavier values (0.12 to 0.38‰), which coincide with the period of intensified steel production and are interpreted as reflecting increasing metallurgical inputs, particularly from Zn-bearing impurities released during iron ore smelting and refining processes (Sonke et al., 2008; Mattielli et al., 2009); and (iii) a marked peak $\delta^{66}Zn_{JMC}$ value of 0.76‰, associated with extremely high Fe contents (32.5 wt% at 47.5 cm depth; Table S2),

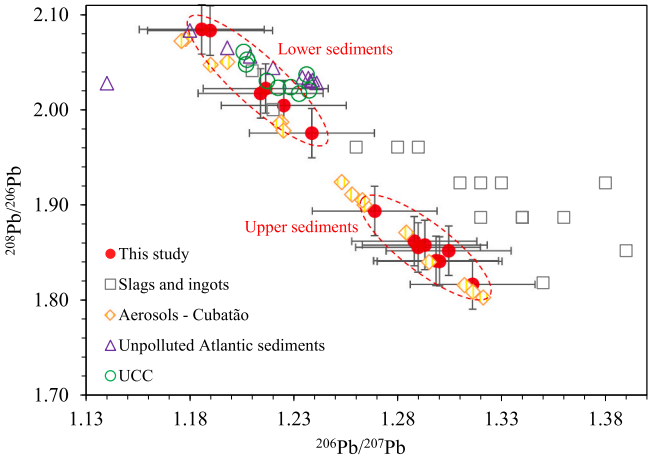

Fig. 4. Plot of $^{208}Pb/^{206}Pb$ versus $^{206}Pb/^{207}Pb$ showing isotopic compositions of upper (0–110 cm) and lower (110–260 cm) sediments from the Morrão River. Error bars for the data from this study represent the standard deviation (2 σ) of the isotopic ratios. The plot includes comparisons with Pb smelter slags and ingots (Rabinowitz, 2002, 2005), industrial aerosols from Cubatão (Souto-Oliveira et al., 2018), unpolluted Atlantic sediments (Barros de Oliveira et al., 2009), and the Upper Continental Crust (UCC; Millot et al., 2004).

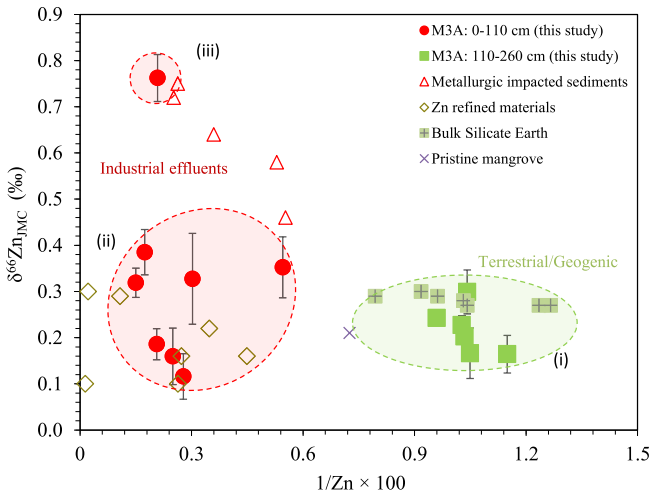

Fig. 5. Plot of $\delta^{66}Zn\_JMC$ versus 1/Zn × 100 for the Morrão River core (M3A), compared with data from metallurgically impacted sediments (Araújo et al., 2017), Zn-refined materials (Sonke et al., 2008; Mattielli et al., 2009), sewage and wastewater (Chen et al., 2009; Garnier et al., 2024), Bulk Silicate Earth (BSE; Chen et al., 2013), and pristine mangrove sediments (Garnier et al., 2024). The figure illustrates the isotopic distinction between natural (i) and industrial (ii, iii) end-members, highlighting the mixed origin of Zn in the studied sediments. Error bars for the data from this study represent the two standard deviations (2σ) of the isotopic ratios.

indicative of a strong metallurgical imprint. Such heavy Zn isotope signatures are comparable to those reported for sediments affected by smelting and metallurgical activities ($\delta^{66}Zn \approx 0.86 \pm 0.15‰$; Araújo et al., 2017), supporting an industrial origin.

The isotopic signatures observed here are supported by experimental and field studies, which indicate that Zn isotope fractionation during iron and steel production typically involves preferential volatilization of lighter isotopes ($\Delta^{66}Zn_{vapor-residue} \approx -0.3$ to $-0.6‰$), leading to enrichment of heavier Zn isotopes in slags, dusts, and effluents discharged to the environment (Sivry et al., 2008; Yin et al., 2015). The broad Zn isotopic range observed in the core likely reflects the combined effects of such high-temperature industrial fractionation prior to deposition and subsequent diagenetic processes, including preferential incorporation of heavier Zn isotopes into Fe-rich phases (Araújo et al., 2017; Garnier et al., 2024). Conversely, the lighter $\delta^{66}Zn_{JMC}$ values observed in the uppermost sediments (~0.12‰ at 2.5 cm depth) are consistent with isotopic signatures reported for untreated urban sewage and wastewater ($\delta^{66}Zn \approx 0.08$ to 0.28‰; Chen et al., 2009; Thapalia et al., 2015; Garnier et al., 2024). Although no direct hydrological measurements or effluent discharge data are available for the study area, the overlap between these values and those reported for urban effluents, together with the reduced metallurgical signal in the most recent layers, suggests an increasing relative contribution from urban sources. This interpretation is therefore considered indicative rather than definitive and highlights the need for complementary hydrological and effluent monitoring to further constrain Zn sources in the system.

5. Conclusions

The Pb and Zn isotopic records preserved in the sedimentary profile reflect the industrial evolution of Cubatão over the past decades. Radiogenic Pb and heavy Zn isotopic signals correspond to the period of uncontrolled industrial emissions (1950s–1970s), while the post-1984 interval, following the implementation of pollution-control policies, is marked by more variable Zn isotopic compositions, indicating diffuse contributions from urban sources. Lead isotopes ($^{206}Pb/^{207}Pb$ and $^{208}Pb/^{206}Pb$) proved to be reliable stratigraphic tracers of the steel plant legacy, effectively distinguishing pre-industrial geogenic sediments from layers influenced by metallurgical emissions. In contrast, Zn isotopes ($\delta^{66}Zn$) provided complementary insight, exhibiting heavy isotope enrichment associated with high-temperature siderurgical processes and lighter signatures indicative of diffuse urban and wastewater contributions following the implementation of emission-control measures. The strong correlations observed between isotopic ratios and Fe content highlight the dual role of Fe-bearing minerals, not only as geochemical barriers but also as active agents of isotopic fractionation in estuarine environments. Overall, this study demonstrates that Pb and Zn isotopes are sensitive tracers of anthropogenic influence in mangrove sediments, capable of detecting contamination signals even when elemental concentrations fail to do so. Their combined application strengthens the reconstruction of contamination histories and provides a robust framework for evaluating the legacy impacts of industrial activities and the long-term resilience of tropical estuarine ecosystems.

CRediT authorship contribution statement

Sanny Castro: Writing – original draft, Visualization, Methodology, Investigation, Conceptualization. **Wanilson Luiz-Silva:** Writing – review & editing, Supervision, Methodology, Investigation, Funding acquisition, Conceptualization. **Hyeryeong Jeong:** Writing – review & editing, Visualization, Methodology, Investigation, Formal analysis, Conceptualization. **João Barreira:** Writing – original draft, Visualization, Methodology, Investigation, Formal analysis, Conceptualization. **Wilson Machado:** Writing – review & editing, Methodology, Investigation, Conceptualization. **Christian Sanders:** Writing – review & editing, Methodology, Investigation, Funding acquisition, Conceptualization. **Jeremie Garnier:** Writing – review & editing, Methodology, Investigation, Funding acquisition, Conceptualization. **Daniel F. Araújo:** Writing – review & editing, Supervision, Methodology, Investigation, Funding acquisition, Formal analysis, Conceptualization.

Declaration of competing interest

The authors declare that they have no known competing financial interests or personal relationships that could have appeared to influence the work reported in this paper.

Acknowledgements

We acknowledge the financial support provided by the São Paulo Research Foundation – FAPESP (Grants No. 04/00059-6 and 2008/11511-8) and the Brazilian National Council for Scientific and Technological Development – CNPq (Grant No. 432922/2016-4). W. Machado acknowledges additional support from CNPq (Grant No. 312849/2019-2), and S. Castro acknowledges support from CNPq (Fellowship No. 140945/2020-2) and the Coordination for the Improvement of Higher Education Personnel (CAPES), Brazil (Grant No. 88887.695501/2022-00).

Appendix A. Supplementary data

Supplementary data to this article can be found online at https://doi.org/10.1016/j.marpolbul.2026.119470.

Data availability

Data will be made available on request.

References

Aily, C., 2001. Caracterização isotópica de Pb na atmosfera: um exemplo da cidade de São Paulo. Dissertação de Mestrado. Instituto de Geociências, Universidade de São Paulo (USP). São Paulo, Brazil. http://www.teses.usp.br/teses/disponiveis/44/44134/tde-11092015-093709/.

Almeida, F.F.M., Carneiro, C.D.R., 1998. Origin and evolution of the Serra Do Mar (Brazilian southeast). Rev. Bras. Geociênc. 28, 135–150. http://bjg.siteoficial.ws/1998/n.2/3.pdf.

Angeli, J.L.F., Sartoretto, J.R., Kim, B.S.M., Ferreira, P.A.L., Mahiques, M.M., Figueira, R. C.L., 2021. Trace element fluxes during the "Anthropocene" in a large south american industrial and port area (Santos and São Vicente estuarine system, SE, Brazil). Environ. Monit. Assess. 193, 594. https://doi.org/10.1007/s10661-021-09378-3.

Araújo, D.F., Boaventura, G.R., Machado, W., Viers, J., Weiss, D., Patchineelam, S.R., Ruiz, I., Rodrigues, A.P.C., Babinski, M., Dantas, E., 2017. Tracing of anthropogenic zinc sources in coastal environments using stable isotope composition. Chem. Geol. 449, 226–235. https://doi.org/10.1016/j.chemgeo.2016.12.004.

Araújo, D.F., Machado, W., Weiss, D., Mulholland, D.S., Garnier, J., Souto-Oliveira, C.E., Babinski, M., 2018. Zinc isotopes as tracers of anthropogenic sources and biogeochemical processes in contaminated mangroves. Appl. Geochem. 95, 25–32. https://doi.org/10.1016/j.apgeochem.2018.05.008.

Araújo, D.F., Ponzevera, E., Briant, N., Knoery, J., Sireau, T., Mojtahid, M., Metzger, E., Brach-Papa, C., 2019. Assessment of the metal contamination evolution in the Loire estuary using Cu and Zn stable isotopes and geochemical data in sediments. Mar. Pollut. Bull. 143, 12–23. https://doi.org/10.1016/j.marpolbul.2019.04.034.

Barros de Oliveira, S.M., Ruiz Pessenda, L.C., Marques Gouveia, S.E., Babinski, M., Favaro, D.I.T., 2009. A geochemical and lead isotopic record from a small pond in a remote equatorial island, Fernando de Noronha, Brazil. Holocene 19, 439–448. https://doi.org/10.1177/0959683608101393.

Borrely, S.I., Garcia, V.S.G., Borrely, T., Fávaro, D.I.T., 2018. Metals, trace elements and ecotoxicity in sediments of the Cubatão River. Brazil. Ecotoxicol. Environ. Contam. 13, 49–61. https://doi.org/10.5132/eec.2018.02.07.

Castro, S., Luiz-Silva, W., Machado, W., Valezio, E., 2021. Mangrove sediments as long-term mercury sinks: evidence from millennial to decadal time scales. Mar. Pollut. Bull. 173, 113031. https://doi.org/10.1016/j.marpolbul.2021.113031.

Chen, H., Savage, P.S., Teng, F.-Z., Helz, R.T., Moynier, F., 2013. Zinc isotope fractionation during magmatic differentiation and the isotopic composition of the bulk earth. Earth Planet. Sci. Lett. 369–370, 34–42. https://doi.org/10.1016/j.epsl.2013.02.037.

Chen, J., Gaillardet, J., Louvat, P., Huon, S., 2009. Zn isotopes in the suspended load of the Seine River, France: isotopic variations and source determination. Geochim. Cosmochim. Acta 73, 4060–4076. https://doi.org/10.1016/j.gca.2009.04.017.

Couto, J.M., 2003. Entre estatais e transnacionais: O pólo industrial de Cubatão. Tese de Doutorado. Instituto de Economia, Universidade Estadual de Campinas, Campinas, Brazil. https://repositorio.unicamp.br/acervo/detalhe/275872.

Cunha, B., Machado, W., Marra, A., Araújo, D., Garnier, J., Martins, A., Saliba, B., Geraldes, M., 2018. Lead source assessment by isotopic and elementary composition in the transition from pristine to polluted condition of coastal sediments. J. Sediment. Environ. 3, 46–53. https://doi.org/10.12957/jse.2018.33890.

Dong, Y., Rosenbaum, R.K., Hauschild, M.Z., 2015. Assessment of metal toxicity in marine ecosystems: comparative toxicity potentials for nine cationic metals in coastal seawater. Environ. Sci. Technol. 50, 269–278. https://doi.org/10.1021/acs.est.5b01625.

Fangwen, W., Zhang, X., Liu, Y., Chen, J., Li, H., 2025. The distribution characteristics of heavy metals and Pb isotopes in the sediments of the Fuhe River, South China. Environ. Res. Commun. 7, ae0b1e. https://doi.org/10.1088/2515-7620/ae0b1e.

Garnier, J., Tonha, M., Araujo, D.F., Landrot, G., Cunha, B., Machado, W., Resongles, E., Freydier, R., Seyler, P., Ratié, G., 2024. Detangling past and modern zinc anthropogenic source contributions in an urbanized coastal river by combining elemental, isotope and speciation approaches. J. Hazard. Mater. 480, 135714. https://doi.org/10.1016/j.jhazmat.2024.135714.

Guo, H., Song, Z., Wang, S., Yan, S., Wang, Y., Gao, Y., Xia, J., 2025. Assessment of heavy metal contamination and ecological risk in mangrove marine sediments inside and outside Zhanjiang Bay: implications for conservation. J. Mar. Sci. Eng. 13, 708. https://doi.org/10.3390/jmse13040708.

Hossain, M.K., Islam, F., Karmaker, K.D., Akhtar, U.S., Parvin, A., Parvin, A., Moniruzzaman, M., Saha, B., Suchi, P.D., Hossain, M.A., Shaikh, M.A.A., 2024. Source-specific geochemical and health risk assessment of anthropogenically induced metals in a tropical urban waterway. Mar. Pollut. Bull. 203, 116483. https://doi.org/10.1016/j.marpolbul.2024.116483.

Hu, B., Cui, R., Li, J., Wei, H., Zhao, J., 2011. Characteristics of heavy metals and Pb isotopic signatures in sediment cores from shallow urban lakes in Nanjing, China. J. Environ. Sci. 23, 1719–1726. https://doi.org/10.1016/j.jenvman.2010.10.016.

Jeong, H., Ra, K., 2021. Multi-isotope signatures (cu, Zn, Pb) of different particle sizes in road-deposited sediments: a case study from industrial area. J. Anal. Sci. Technol. 12, 1–14. https://doi.org/10.1186/s40543-021-00292-4.

Jeong, H., Ra, K., Choi, J.Y., 2021. Copper, zinc and Lead Isotopic Delta values and isotope ratios of various geological and biological reference materials. Geostand. Geoanal. Res. 45, 551–563. https://doi.org/10.1111/ggr.12379.

Jeong, H., Araújo, D.F., Knœry, J., Briant, N., Ra, K., 2023. Isotopic (cu, Zn, and Pb) and elemental fingerprints of antifouling paints and their potential use for environmental forensic investigations. Environ. Pollut. 322, 121176. https://doi.org/10.1016/j.envpol.2023.121176.

Junqueira, T.P., Araújo, D.F., Jeong, H., Guatame-Garcia, A., Pascoe, T., Harrison, A.L., Leybourne, M.I., Smol, J.P., Vriens, B., 2024. Spatiotemporal and multi-isotope assessment of metal sedimentation in the Great Lakes. Environ. Res. 253, 119176. https://doi.org/10.1016/j.envres.2024.119176.

Klumpp, A., Klumpp, G., Domingos, M., Silva, M.D., 1996. Fluoride impact on native tree species of the Atlantic Forest near Cubatão, Brazil. Water Air Soil Pollut. 87, 57–71. https://doi.org/10.1007/BF00696829.

Komárek, M., Ettler, V., Chrastný, V., Mihaljevič, M., 2008. Lead isotopes in environmental sciences: a review. Environ. Int. 34, 562–577. https://doi.org/10.1016/j.envint.2007.10.005.

Krupnova, T., Rakova, O., Udachin, V., Gavrilkina, S., Bondarenko, K., 2023. Isotopic ratios as a tool for studying sources of copper, lead, and zinc in natural and urban environments: a review. GEOMATE J. 25, 33–41. https://geomatejournal.com/geomate/article/view/3658.

Kubeneck, L.J., Lenstra, W.K., Malkin, S.Y., Conley, D.J., Slomp, C.P., 2021. Phosphorus burial in vivianite-type minerals in methane-rich coastal sediments. Mar. Chem. 231, 103948. https://doi.org/10.1016/j.marchem.2021.103948.

Lonsdale, J.A., Leach, C., Parsons, D., Barkwith, A., Manson, S., Elliott, M., 2022. Managing estuaries under a changing climate: a case study of the Humber estuary. UK. Environ. Sci. Policy 134, 75–84. https://doi.org/10.1016/j.envsci.2022.04.001.

Luiz-Silva, W., Matos, R.H.R., Kristosch, G.C., Machado, W., 2006. Variabilidade espacial e sazonal da concentração de elementos-traço em sedimentos do sistema estuarino de Santos-Cubatão (SP). Quim Nova 29, 256–263. https://doi.org/10.1590/S0100-40422006000200016.

Luiz-Silva, W., Machado, W., Matos, R.H., 2008. Multi-elemental contamination and historic record in sediments from the Santos-Cubatão estuarine system, Brazil. J. Braz. Chem. Soc. 19, 1490–1500. https://doi.org/10.1590/S0103-50532008000800008.

Machado, W., Sanders, C.J., Santos, I.R., Sanders, L.M., Silva-Filho, E.V., Luiz-Silva, W., 2016. Mercury dilution by autochthonous organic matter in a fertilized mangrove wetland. Environ. Pollut. 213, 30–35. https://doi.org/10.1016/j.envpol.2016.02.002.

Mahiques, M.M., Hanebuth, T.J., Martins, C.C., Montoya-Montes, I., Alcántara-Carrió, J., Figueira, R.C., Bícego, M.C., 2016. Mud depocentres on the continental shelf: a neglected sink for anthropogenic contaminants from the coastal zone. Environ. Earth Sci. 75, 1–12. https://doi.org/10.1007/s12665-015-4782-z.

Mattielli, N., Petit, J.C., Deboudt, K., Flament, P., Perdrix, E., Taillez, A., Rimetz-Planchon, J., Weis, D., 2009. Zn isotope study of atmospheric emissions and dry depositions within a 5 km radius of a Pb–Zn refinery. Atmos. Environ. 43, 1265–1272. https://doi.org/10.1016/j.atmosenv.2008.11.030.

Millot, R., Allègre, C.J., Gaillardet, J., Roy, S., 2004. Lead isotopic systematics of major river sediments: a new estimate of the Pb isotopic composition of the upper continental crust. Chem. Geol. 203, 75–90. https://doi.org/10.1016/j.chemgeo.2003.09.002.

Obrist, D., Kirk, J.L., Zhang, L., Sunderland, E.M., Jiskra, M., Selin, N.E., 2018. A review of global environmental mercury processes in response to human and natural perturbations: changes of emissions, climate, and land use. Ambio 47, 116–140. https://doi.org/10.1007/s13280-017-1004-9.

Olivo, G.R., Gauthier, M., Gariepy, C., Carignan, J., 1996. Transamazonian tectonism and au–Pd mineralization at the Cauê mine, Itabira District, Brazil: Pb isotopic evidence. J. S. Am. Earth Sci. 9, 273–279. https://doi.org/10.1016/0895-9811(96)00013-2.

Perrotta, M.M., Salvador, E.D., Lopes, R.C., D'Agostino, L.Z., Peruffo, N., Gomes, S.D., Sachs, L.L.B., Meira, V.T., Garcia, M.G.M., 2005. Mapa geológico do Estado de São Paulo, escala 1:750.000. CPRM – Serviço Geológico do Brasil, São Paulo, Brazil. https://rigeo.sgb.gov.br/bitstream/doc/2966/5/mapa_geologico.pdf?utm_source=chatgpt.com.

Pontér, S., Sutliff-Johansson, S., Engström, E., Widerlund, A., Mäki, A., Rodushkina, K., Rodushkin, I., 2020. Evaluation of a multi-isotope approach as a complement to concentration data within environmental forensics. Minerals 11, 37. https://doi.org/10.3390/min11010037.

Rabinowitz, M.B., 2002. Isotopic characterization of various brands of corroding grade refined lead metal. Bull. Environ. Contam. Toxicol. 69, 471–478. https://doi.org/10.1007/s00128-002-0090-x.

Rabinowitz, M.B., 2005. Lead isotopes in soils near five historic American lead smelters and refineries. Sci. Total Environ. 346, 138–148. https://doi.org/10.1016/j.scitotenv.2004.11.021.

Salomons, W., Förstner, U., 1984. Sediments and the transport of metals. In: Metals in the Hydrocycle. Springer, Berlin, Heidelberg, pp. 63–98. https://doi.org/10.1007/978-3-642-69325-0_3.

Sanders, C.J., Eyre, B.D., Santos, I.R., Machado, W., Luiz-Silva, W., Smoak, J.M., Breithaupt, J.L., Ketterer, M.E., Sanders, L., Marotta, H., Silva-Filho, E., 2014. Elevated rates of organic carbon, nitrogen, and phosphorus accumulation in a highly impacted mangrove wetland. Geophys. Res. Lett. 41, 2475–2480. https://doi.org/10.1002/2014GL059789.

Sivry, Y., Riotte, J., Sonke, J.E., Audry, S., Schäfer, J., Viers, J., Dupré, B., 2008. Zn isotopes as tracers of anthropogenic pollution from Zn-ore smelters The Riou Mort–Lot River system. Chem. Geol. 255, 295–304. https://doi.org/10.1016/j.chemgeo.2008.06.038.

Sonke, J.E., Sivry, Y., Viers, J., Freydier, R., Dejonghe, L., André, L., Dupré, B., 2008. Historical variations in the isotopic composition of atmospheric zinc deposition from a zinc smelter. Chem. Geol. 252, 145–157. https://doi.org/10.1016/j.chemgeo.2008.02.006.

Souto-Oliveira, C.E., Babinski, M., Araújo, D.F., Andrade, M.D.F., 2018. Multi-isotopic fingerprints (Pb, Zn, cu) applied for urban aerosol source apportionment and discrimination. Sci. Total Environ. 626, 1350–1366. https://doi.org/10.1016/j.scitotenv.2018.01.192.

Sun, G.-X., Wang, X.-J., Hu, Q.-H., 2011. Using stable lead isotopes to trace heavy metal contamination sources in sediments of Xiangjiang and Lishui Rivers in China. Environ. Pollut. 159, 3406–3410. https://doi.org/10.1016/j.envpol.2011.08.037.

Tang, H., Ke, Z., Yan, M., Wang, W., Nie, H., Li, B., Wang, J., 2018. Concentrations, distribution, and ecological risk assessment of heavy metals in Daya bay, China. Water 10, 780. https://doi.org/10.3390/w10060780.

Thapalia, A., Borrok, D.M., Van Metre, P.C., Wilson, J., 2015. Zinc isotopic signatures in eight lake sediment cores from across the United States. Environ. Sci. Technol. 49, 132–140. https://doi.org/10.1021/es5036893.

Todt, W., Cliff, R.A., Hanser, A., Hofmann, A.W., 1996. Recalibration of NBS lead standards using a 207Pb-204Pb double spike. Terra Nova 8, 384–392.

Volpato, J., 2015. Relação entre geoquímica e minerais (Magnetita, Hematita, Pirita e Vivianita) em sedimentos estuarinos contaminados, Santos (SP). Dissertação de Mestrado. Universidade Estadual de Campinas (UNICAMP), Campinas. https://doi.org/10.47749/T/UNICAMP.2015.948298.

Yin, R., Feng, X., Chen, B., Zhang, J., Wang, W., Li, X., 2015. Identifying the sources and processes of mercury in subtropical estuarine and ocean sediments using hg isotopic composition. Environ. Sci. Technol. 49, 1347–1355. https://doi.org/10.1021/es504070y.

Yu, Y., Li, Y., Li, B., Ren, Y., Dong, X., 2021. Identification and quantification of lead source in sediment in the northern East China Sea using stable lead isotopes. J. Oceanol. Limnol. 39, 1887–1900. https://doi.org/10.1007/s00343-020-0286-0.